B-10-635 #10

HIGH PERFORMANCE PHOTODIODES

Final Report for Project A-4233

Prepared for

Dr. William T. Vetterling
Microelectronics/Materials Center
Polaroid Corporation
21 Osborn Street, Dept. 775
Cambridge, MA 02139

Prepared by

Dr. Christopher J. Summers
Georgia Tech Microelectronics Research Center
Georgia Institute of Technology
Atlanta, Georgia 30332

April 1995

TABLE OF CONTENTS

Page

1. INTRODUCTION 1

2. PROGRESS 3

3. RESULTS 5

4. CONCLUSIONS 17

5. REFERENCES 18

APPENDIX I: FABRICATION PROCEDURES FOR SL AVALANCHE PHOTODIODES 19

1. Ohmic Contact Fabrication 19
2. Mesa Fabrication 20
3. Via Hole Fabrication 21

APPENDIX II: CHARACTERIZATION OF THE SL APD'S 24

1. Introduction 24

A. Description of the Optical Apparatus 24
B. Description of the Electrical Circuit 26
C. Description of the Instruments 30

2. Calibration of the Measurement Circuit 31

A. I-V Measurements and Multiplication Gain Calculation 31
B. Calibration of Entire Measurement Circuit 31
C. Calibration Using a Si PIN Photodiode 35

3. Theory of the Measurements 38

A. I-V Measurements and Multiplication Gain Calculation 38
B. Determination of the Excess Noise Factor 39
C. Quantum Efficiency Measurements 42

1. INTRODUCTION

The objective of this program was to develop a very low noise solid state diode detector which could be applied to a broad range of Polaroid activities, including light metering, detection of fluorescent emission (biomedical applications), optical disk or card reading (or tracking), and high-sensitivity camera applications when incorporated into array structures.

In this program multiple quantum well structures were used to design high performance APDs because of their potential to minimize the excess noise in the avalanche process. Low noise is achieved if the ionization rates of the electrons and the holes, α and β respectively, are greatly different, equivalently α/β (or β/α) is high. Since the presentation of the original idea by Chin et al (1980) and the first experimental investigations by Capasso et al (1982A), several novel designs have been proposed: the doped multilayer APD (1982), the staircase APD (1982b), the channeling APD (1983), the pn-doped homojunction and heterojunction APD (1986) (or doped barrier APD) and the doped quantum well APD (1990). It is predicted that the last two designs could lead to the first solid state photomultiplier APD where the avalanche excess noise has been totally suppressed.

In this program quantitative experimental investigations of several AlGaAs/GaAs multiple-quantum-well avalanche photodiode (APD) structures, the superlattice APD, the doped barrier APD and the doped quantum well APD are reported. Only diodes exhibiting

self consistent C-V, I-V and breakdown voltage characteristics were investigated and showed strong agreement between electron- and hole-ionization rates, as determined from gain and noise measurements, respectively. This study provides new data on the performance of doped barrier and quantum well APDs and establishes a comparison with the electron- and hole-ionization rates for $Al_xGa_{1-x}As$/GaAs MQW-APDs. These devices exhibit gains of ~ 20 with excess-noise factors <5 at bias voltages <10V. Thus significant results were obtained on both conventional AlGaAs/GaAs superlattice APD's and barrier-doped superlattice APDs. Preliminary data was also obtained on some delta-doped quantum well devices. Additionally, it should be noted that this excess noise factor is within 18% of the value given for a Hamamatsu Si avalanche photodiode detector and demonstrates the high potential of these concepts. Progress was also made in developing better models and insight into device operation. However, further work remains to be done on resolving the differences between experiment and the theoretical predictions which ideally suggest that a further two orders of magnitude improvement is possible.

The success of this effort was based on developing a stable and reproducible material growth and device fabrication technology and the setting up of the equipment and a dedicated electromagnetic shielded room to perform very sensitive gain and noise measurements on advanced APD structures. Full details of the work on device fabrication, evaluation, and results are described in appendices I and II, respectively.

2. PROGRESS

This report presents detailed investigations on undoped MQW APDs having different geometries and aluminum compositions, doped barrier and doped well APDs. A comprehensive self-consistent methodology was used where current-voltage, capacitance-voltage, doping profile, and noise characteristics were extensively analyzed.

2. EXPERIMENTAL

The structures were grown by molecular beam epitaxy. Growth was initiated on an n^+ Si doped substrate followed by a short period superlattice to prevent propagation of dislocations and impurities. All the device structures were PINs where the I region was composed of the MQW structure with P and N contact layers of 1 μm and 1.5 μm doped to 1 x 10^{18} cm^{-3} with Be and Si, respectively. The MQW structures had 25 $Al_xGa_{1-x}As$/GaAs multilayers with aluminum compositions of 0.30, 0.35 and 0.45. The aluminum composition, x, of the AlGaAs layers was calibrated using photoluminescence measurements. The samples showed high exciton recombination photoluminescence intensities with a half width of 5 mev. Growth interruption techniques were used to obtain well defined pn doped regions in the MQW structures. The dopant concentration was calibrated by Hall effect and was kept below 6 x 10^{18} cm^{-3} to limit dopant diffusion.

The devices were fabricated into 2 x 10^{-4} cm^{-2} area mesa

structures using standard photolithography techniques (Appendix I). The device configuration allows for electron or hole injection because both p^+ and n^+ layers can be illuminated. Precise control of the growth and fabrication procedures yields identical photodiode characteristics on the same wafer and from one run to another. A SiO_2 dielectric coating suppressed surface leakage currents and provided devices with very low dark currents. The photodiode characterization consisted of computer automated I-V, C-V and noise measurements. The dc I-V characteristics were measured in the dark and under illumination by a HeNe laser light with a 5 μm diameter spot. The photocurrent gain was calculated from the increase of the unmultiplied photocurrent and was verified to be independent of the light intensity. The C-V measurements were made on a LCZ meter between 80 Khz and 1 Mhz and at 300 K and 77 K. The apparent free carrier concentration profile was obtained from differentiation of the C-V data. Noise measurements consisted of measuring the variance of the photodiode output current for different gains. Absolute noise measurements were performed using a spectrum analyzer tuned to a frequency of 200 Khz. Several noise sources were used to calibrate the system and the noise measurements are accurate to within a few percent.

3. RESULTS

3.1 Undoped MQW APDs

Investigations were first performed on 2.5 μm thick MQW $Al_xGa_{1-x}As/GaAs$ structures with different well and barrier widths, L_B and L_Z respectively, and with a constant MQW period width of 1000 Å. The values of L_Z studied were: 200 Å, 350 Å, 500 Å, 650 Å and 800 Å. A 400 Å thick spacer layer was added prior to the first well on the P^+ contact side and also prior to the first barrier on the N^+ contact side to avoid trapped carriers at the first heterojunction for electric fields above 100 kV/cm. The MQW structures have an Al composition, x, of 0.3, 0.35 and 0.43. Typical dark I-V characteristics are shown in Figure 1 for electron injection. The dark current was below 10 nA at 80 % of the breakdown voltage for x = 0.30 and below 1 nA for x = 0.43. The dark current decreased with decreasing well width, and with increasing x.

The photocurrent increases slowly with the applied voltage, becomes constant between 25-35 V and finally increases exponentially above 50 V. As also shown in Figure 1, the breakdown voltage, V_B, increased from 70 to 85 V as the barrier width increased from 200 Å to 800 Å. For a given geometry and Al composition, V_B is constant within 2 % for all photodiodes tested, and increases as the Al composition increases. Similarly, I-V measurements were taken for hole injection. These results indicate that the dark current is due to the generation-recombination of

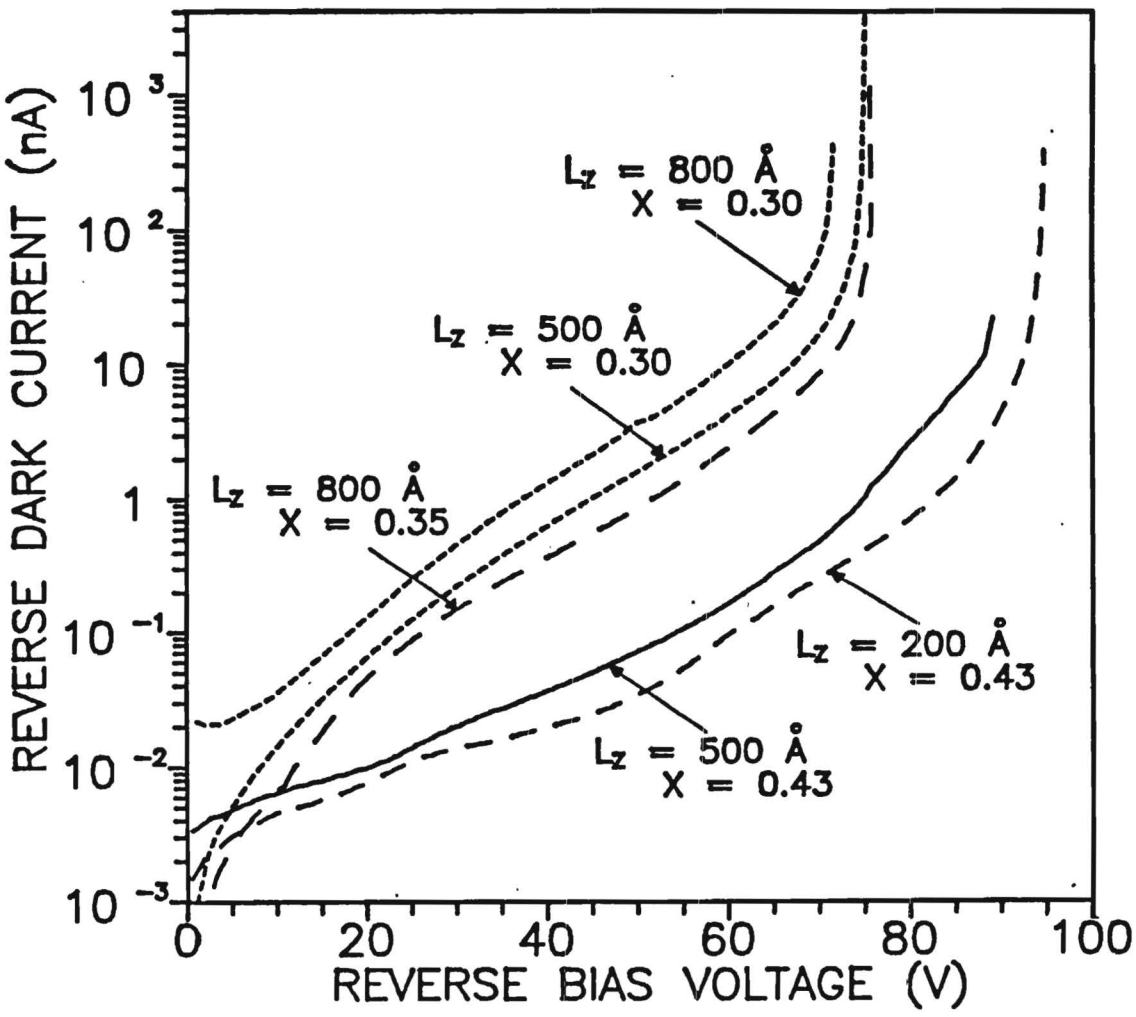

Figure 1. Typical Dark I-V Characteristics for Undoped $Al_xGa_{1-x}As/GaAs$ MQW APDs.

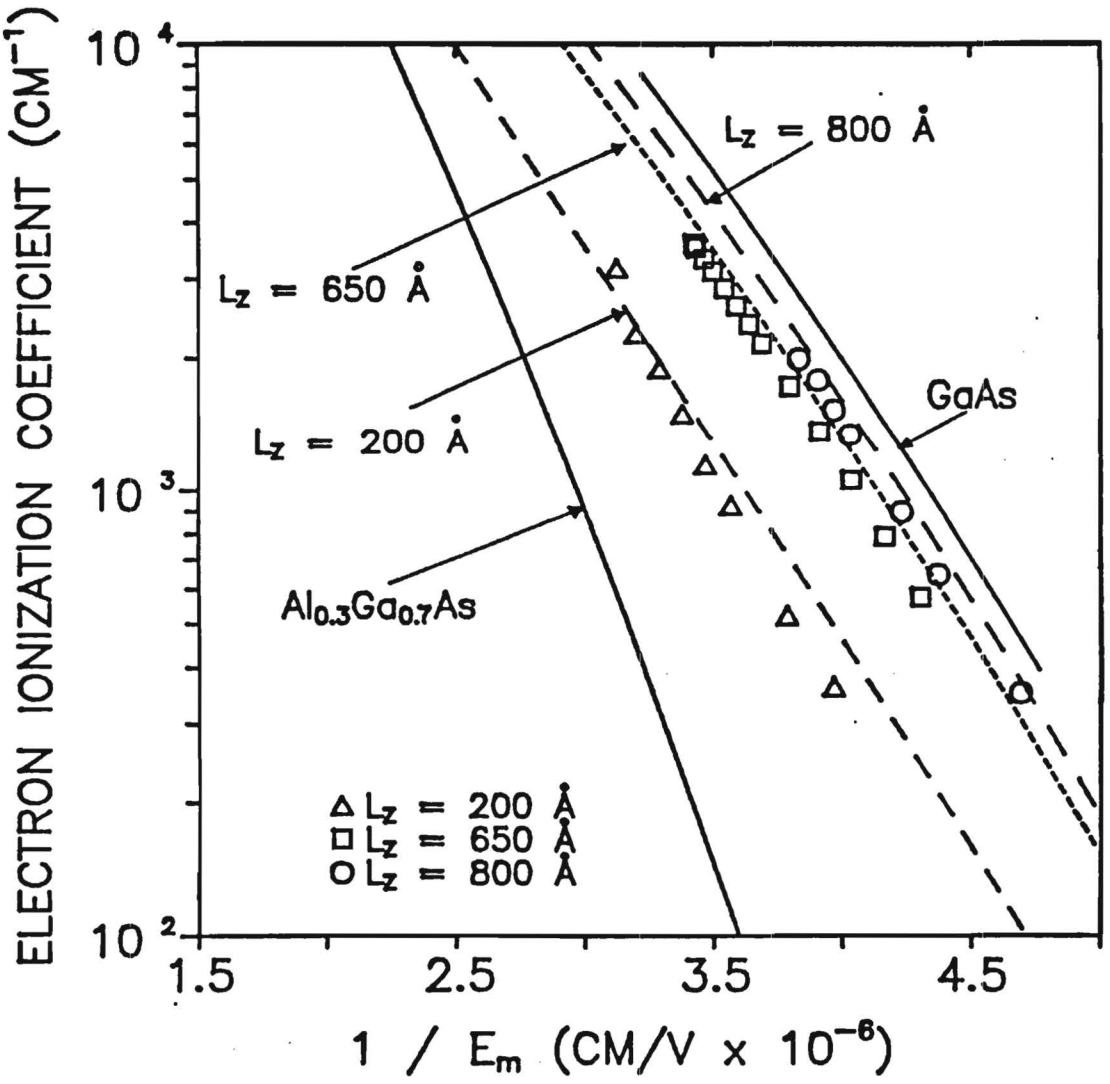

Figure 2. α_{MQW} for $Al_{0.3}Ga_{0.7}As$/GaAs MQW APDs.

conduction band edge discontinuity does not contribute to the enhancement of the electron ionization since α_{MQW} is not enhanced over its value in the bulk GaAs.

The results indicate also that for a higher Al composition, α_{MQW} stays in the same range [300-4000 cm^{-1}], but the corresponding range of electric fields is shifted to higher values. As x increases, the value of E_m at which multiplication starts is increased from 222 Kv/cm for x = 0.30 to 315 Kv/cm for x = 0.42. Consequently, as x increases, the breakdown voltage increases. This is indicated in Figure 3 by a translation of the data to higher electron field values. These results show that the AlGaAs layer of the MQW is "inactive" for x values of 0.30. However, for x = 0.43, the AlGaAs layer appears to reduce the average kinetic energy of the electrons which enter the GaAs layer since the device operates under higher applied electric fields. This energy loss is due to scattering in the X-band of the AlGaAs layer which increases exponentially with the Al composition.

The ratio $k_{MQW}(E_m) = \alpha_{MQW}(E_m)/\beta_{MQW}(E_m)$ increased from 1.72 to 2.5 when the electric field increased from 220 Kv/cm to 280 Kv/cm for the 5 geometries studied and x = 0.30. However $k_{MQW}(E_m)$ was reduced to a constant k = 2.5 for x = 0.43. The results agree with the predicted value using the relation $k_{MQW}(E_m) = \alpha_{AV}(E)/\beta_{AV}(E)$ for x = 0.30, but fail for x = 0.43 since the ratio obtained from the measurements is lower. These results indicate that both the electron and hole average energy are reduced due to the AlGaAs

layer. The hole average energy is reduced by a larger amount since MQW structures with x = 0.43 give a higher k value.

Noise measurements indicate a k value (McIntyre 1966) between 1.7 and 2.5 for the x = 0.30 MQW and between 2.5 and 3.3 for the x = 0.43 MQW. Results for F_e are plotted versus M_e in Figure 3 for the 200 Å well MQW APD having x = 0.30 and 0.43. The solid lines correspond to the theoretical curves of McIntyre. These results agree with the k_{MQW} obtained from the coefficients $\alpha_{MQW}(E_m)$ which were calculated separately using the electron and hole gain measurements and demonstrate that the characterization techniques are self-consistent.

3.2 Doped MQW APDs: the pn junction doped barrier and doped well APDs.

The doped barrier APD was designed with the same unit cell as the undoped MQW APD and consists of a 800 Å barrier, 200 Å well $Al_{0.35}Ga_{0.65}As/GaAs$ MQW structure where a p^+n^+ equally doped junction was built in the barrier prior to the GaAs well. The fully depleted 150 Å p^+/150 Å n^+ junction, doped at 3 x 10^{18} cm^{-3}, locally enhances the electric field of the MQW structure by superimposing 0.5 eV on the MQW band potential.

The I-V characteristics indicate a low dark current and a low breakdown voltage of about -10 V. C-V characteristics indicate that the photodiode capacitance is higher (15 Pf) than measured for the MQW APD (0.9 Pf) and decreases for increasing diode bias voltage as for a one sided abrupt pn^+ junction. The free carrier

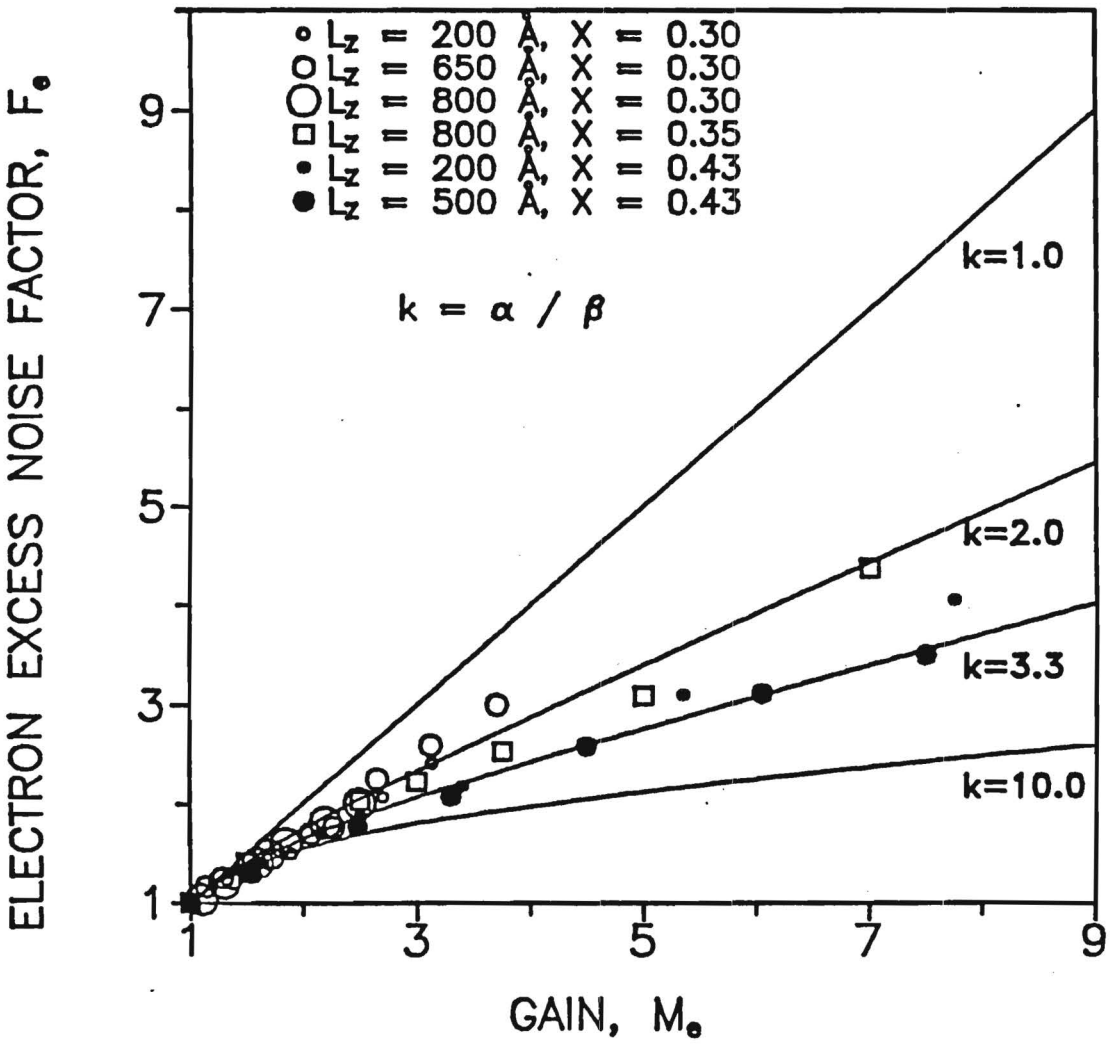

Figure 3. Electron Excess Noise Versus Gain for Undoped MQW APDs.

concentration profile obtained from the analysis of the C-V data is presented in Figure 4. This modeling shows that only one period of the MQW structure is fully depleted at zero bias due to unbalanced doping concentrations in the 300 Å thick junctions. As the field is increased, the depletion width punches through the highest doped side of the 300 Å thick junction to deplete the second period and pn junction of the MQW structure. The results confirm that the depletion region is located close to the P^+ contact thus indicating that $p^+ << n^+$ in the 300 Å thick pn junctions. This is due to the difficulty of achieving equal p- and n- type dopant concentrations in the AlGaAs layer by using solid dopant sources. Although a qualitative variation of the electric field E is predicted, precise calculations of E are not available at present. This α and β can not be obtained separately from the gain measurements. Noise measurement results are presented in Figure 5 were F_e is plotted versus M_e and show that F_e is low for gains up to 5 with a corresponding k between 12.5 and 50. As M_e increases, F_e also increases with a corresponding K between 5 and 10.

The results indicate that k is reduced at low applied electric fields. Since the peak of the electric field is located prior to the well, the injected electrons are more likely to ionize in the well. However, holes generated from ionizations in the well travel in the opposite direction and enter the AlGaAs layer where their ionization probability is smaller compared to the ionization probability of the electrons in GaAs. consequently, α is greatly different from β and a noise reduction is observed. However, K

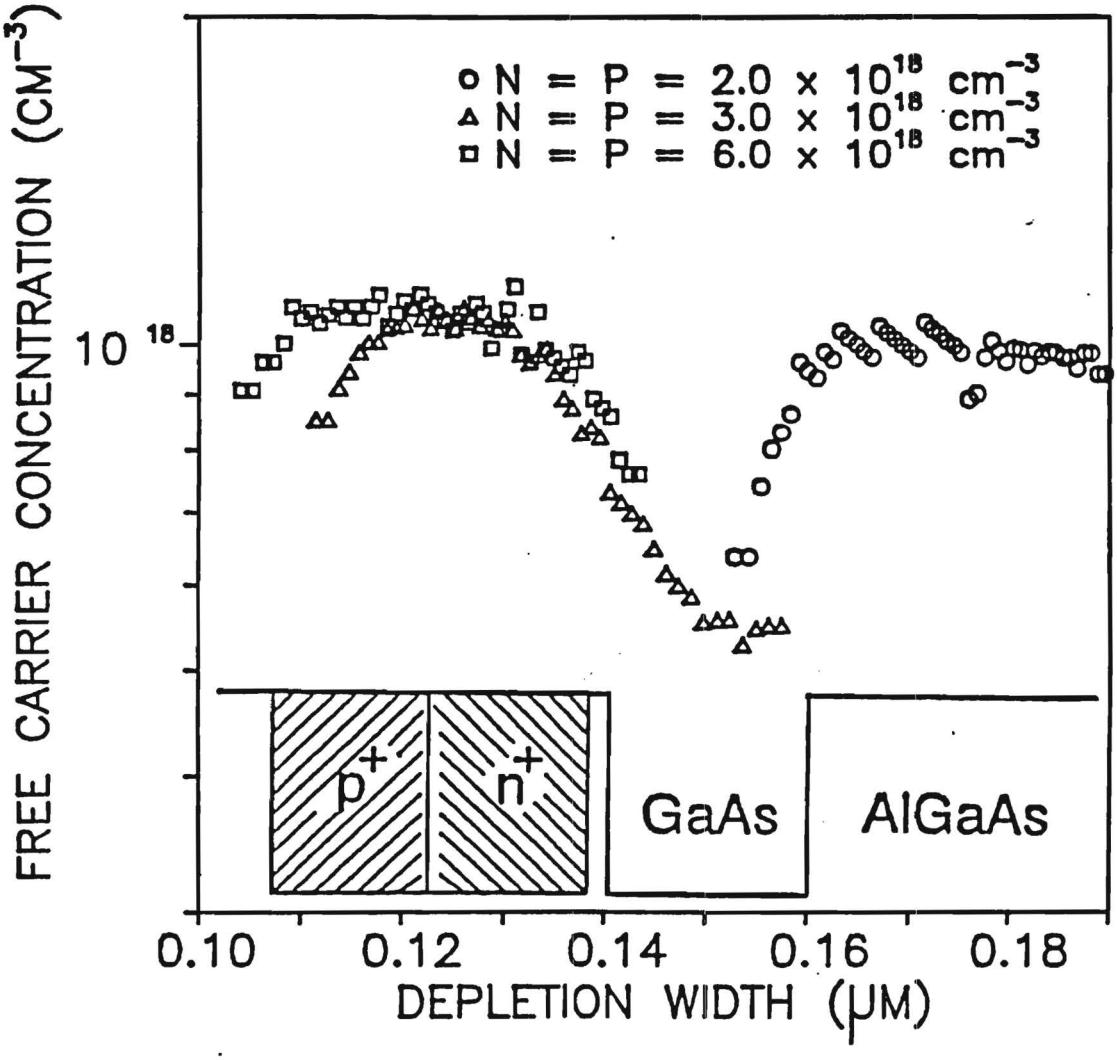

Figure 4. Apparent Free Carrier Concentration of Doped Barrier APDs.

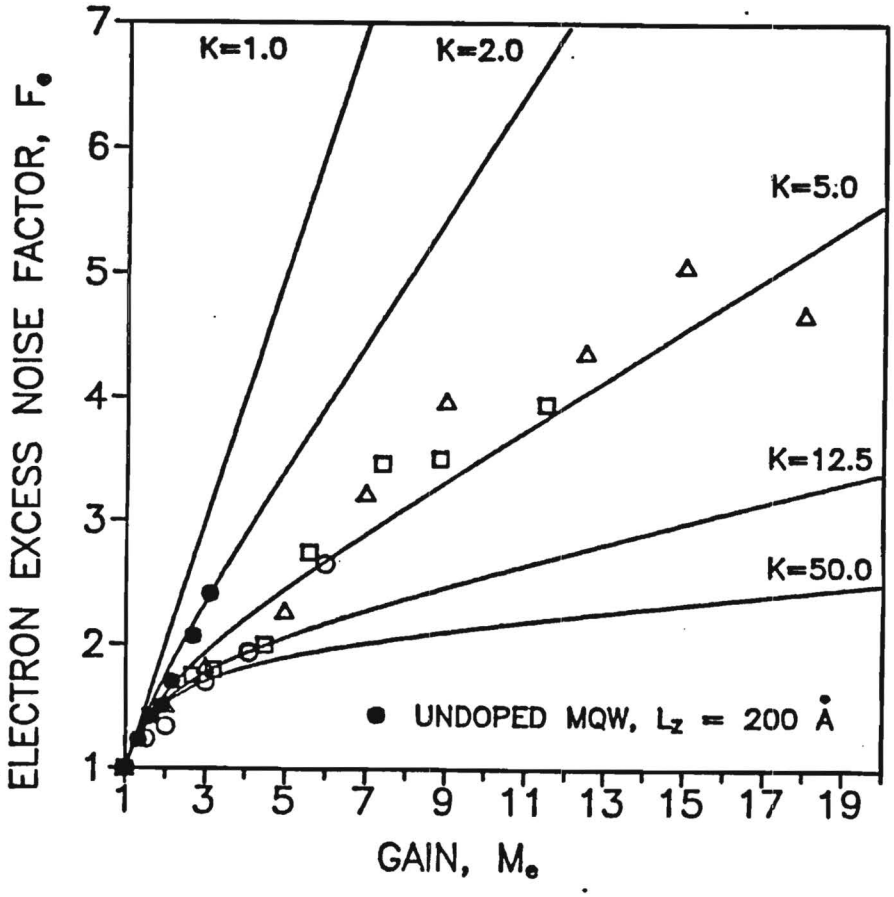

Figure 5. Electron Excess Noise Factor vs Gain, the Solid Circles are for the MQW APD, L_z = 200 Å, and the Open Symbols for the Doped Barrier APD.

increases at higher gain indicating that the hole ionization probability is no longer small compared to the electrons and the applied electric field is high enough to supply kinetic energy to the holes to impact ionize in the following well.

Similar results were obtained for a doped 500 Å well/500 Å barrier $Al_{0.43}Ga_{0.57}As$/GaAs MQW structure where a 300 Å thick pn junction was grown into the well immediately following the barrier. I-V and C-V measurements show that 2 to 3 periods were depleted when the bias voltage was increased from 0 to -12 V at the avalanche breakdown, for these structures high gains up to 400 were obtained. Noise measurements give a similarly low k value as reported for the doped barrier APDs. These results indicate that α/β is enhanced, consequently the noise is reduced, but no information was obtained on the separate magnitude of α and β. The comparable noise performance of both designs suggests that the location of the pn junctions, either in AlGaAs or GaAs material, has little consequence as long as the other parameters of the MQW remain constant (L_2 = 200 Å, L_B = 500 Å). However, the two designs have some differences in their characteristics since the gain is 10 times greater for the doped well than for the doped barrier APD. Further studies are needed to explain this difference.

4. CONCLUSION

The investigations of undoped $Al_xGa_{1-x}Ga/GaAs$ MQW APDs show that α_{MQW} is not enhanced over its value in the bulk materials. Since $\alpha_{GaAs} >> \alpha_{AlGaAs}$, α_{MQW} in the MQW is obtained from an average calculation of the bulk values of low x values, x = 0.3. This, $K_{MQW} = \alpha_{MQW}(E)/\beta_{MQW}(E)$ is between 1.72 and 2.5 which is higher than for GaAs in the same electric field range (k = 1.6). For higher Al composition, x = 0.43, higher electric fields are required for impact ionization. This indicates that both the electron and hole average kinetic energy is reduced due to the AlGaAs layer. However, low k values indicate a noise reduction. Even though the ratio α_{MQW}/β_{MQW} is enhanced, α_{MQW} is not enhanced over its value in the bulk GaAs material. These results have been demonstrated using self-consistent measurement and analysis techniques since similar values of α/β were obtained from gain and noise measurements.

Results on doped barrier and doped well MQW APDs show that the noise of the doped structures is always lower than for the undoped structure having the same geometry. The noise reduction is due to a local enhancement of the built-in potential which confines the electron ionization in the GaAs well. High k values between 12.5 and 50 were obtained for gains up to 5, and values between 5 and 10 for gains above 5. These new designs provide low noise, low breakdown voltage and high gain as required for optoelectronic applications.

5. REFERENCES

1. Blauvelt H., Margalit S. and Yariv A., 1982, Electron. Lett. **18** 375.
2. Brennan K., 1986 IEEE Trans. Electron Dev. **ED-33** 1683.
3. Brennan K. and Vetterling, W.T., 1990 IEEE Trans. Electron Dev. **37** 536.
4. Bulman, G.E., Robbins, V.M., Brennan, K., Hess, K. and Stillman, G.E., 1983, IEEE Trans. Electron Dev. **EDL-4** 181.
5. Capasso, F., Tsang, W.T., Hutchinson, A.L. and Williams, G., 1982a Appl. Phys. Lett. **40** 38.
6. Capasso F., Tsang, W.T., Hutchinson, A.L. and Foy, P., 1982b, Conf. Ser.-Inst. Phys. **63** 473.
7. Capasso, F., Tsang, W.T. and Williams, G.P., 1983, IEEE Trans. Electron Dev. **ED-30** 381.
8. Capasso, F., 1985 Semiconductors and Semimetals - ed R.K. Willardson and A.C. Beer (New York:Wiley) p. 121.
9. Chin, R., Holoniak, N., Stillman, G.E., Tsang, J. and Hess, K., 1982, Appl. Phys. Lett. **16** 467.
10. McIntyre, R.J., 1966, IEEE Trans. Electron Dev. **ED-13** 164.
11. Robbins, V.M., Smith, S.C. and Stillman, G.E., 1988, Appl. Phys. Lett. **52** 296.

APPENDIX I

FABRICATION PROCEDURES FOR SL AVALANCHE PHOTODIODES

New processing techniques have been developed to yield repeatable results and high performance devices. A reliable processing is necessary to insure that materials characteristics are being measured and not artifacts of the processing.

A six level mask is used to fabricate devices having mesa sizes of 75, 100, 130, 200 micron. These different steps include

1. P^+ Contact,
2. Contact Gold Plating,
3. Mesa Fabrication,
4. N^+ Contact,
5. Passivation,
6. Via Hole Fabrication

The ohmic contact and mesa fabrication have been reworked because it has been observed that the details of these processes significantly influence the device performance. The last step, the via hole formation has been developed during the last year. This feature permits the backside illumination of the photodiode and, thus, the characterization of both electron and hole injection modes.

1. Ohmic Contact Fabrication

The emphasis in the ohmic contact work has been to avoid metal diffusion in the window area of the photodiode and to improve the

contact resistance values. Both the p^+- and n^+- contacts were, deposited using a chlorobenzene assisted lift-off process. Since the metal was not deposited on the top window, the metal diffusion was limited to underneath the contact areas only. Thus, the contact area was well defined and the top window material had a better morphology. The p^+ contact was made using 400Å of AuZn and 1000Å of Au. Alloy time and alloy temperature have been optimized to achieve a low contact resistance, R_c. With a p-layer doping level between 10^{17} and 10^{18} cm^{-3}, an average contact resistance of 0.2 ohm·mm was obtained. The alloy was made in a diffusion oven at 400° for 4 minutes in a forming gas environment. The n^+ contact was made using 500Å of AuGe, 100Å of Ni, and 800Å of Au and was alloyed at 375° for 3 minutes. With an n- layer doping level of 10^{18} cm^{-3}, an average contact resistance of 0.07 ohm·mm was obtained.

2. Mesa Fabrication

The mesa etch is a critical step in the device fabrication because it impacts how well the device is defined and also strongly influences the electrical and optical properties of the photodiode. The mesa etch has to preserve the surface morphology of the GaAs to insure success in the N ohmic contact fabrication which is the following step in the processing of the photodiode. In addition, the mesa wall profile has to be smooth to insure a low leakage current.

Etching GaAs is very delicate because of the crystalline

nature of the GaAs lattice. Many GaAs etchants lead to anisotropic etching, because the etch rate depends on the crystal orientation. The etchant currently used is a phosphoric acid based etchant composed of phosphoric acid, hydrogen peroxide as oxidant and methanol as solvent in the ration 1:1:3. Several parameters had to be optimized to have the mesa shape required. These parameters include the temperature of the solution and the agitation motion to insure an etch rate of 2 micron per minute, a minimum undercut, and a repeatable process. The present etching technique yields a leakage current of 1 nA at 90% of the breakdown voltage for most of the SL structures.

3. Via Hole Fabrication

The backside fabrication was composed of two steps: the backside preparation and the via hole etch. In the first step, the wafer was thinned from 250 micron to 75 micron using lapping and polishing techniques. In the second step, the via hole pattern was aligned with the top side of the device using an infrared mask aligner model MJB3 from Karl Suss. The via hole was etched using wet etching techniques. The etching solution was sprayed on the wafer to uniformly etch all the holes on the wafer. The bottom of the via hole is defined by an etch stop layer of AlGaAs ($x>0.5$). Unfortunately, the selective etching of GaAs is a slow process, incompatible with removing 70 micron of material in a short period of time. To solve this problem, 60 micron of GaAs was first removed using a phosphoric acid based etchant which etches GaAs

uniformly at a rate of 4 micron per minute. Then, a selective etchant was used to removed the remaining few microns to stop uniformly at the AlGaAs layer. The solution used was composed of hydrogen peroxide neutralized to a pH of 7 with a few drops of ammonium hydroxide.

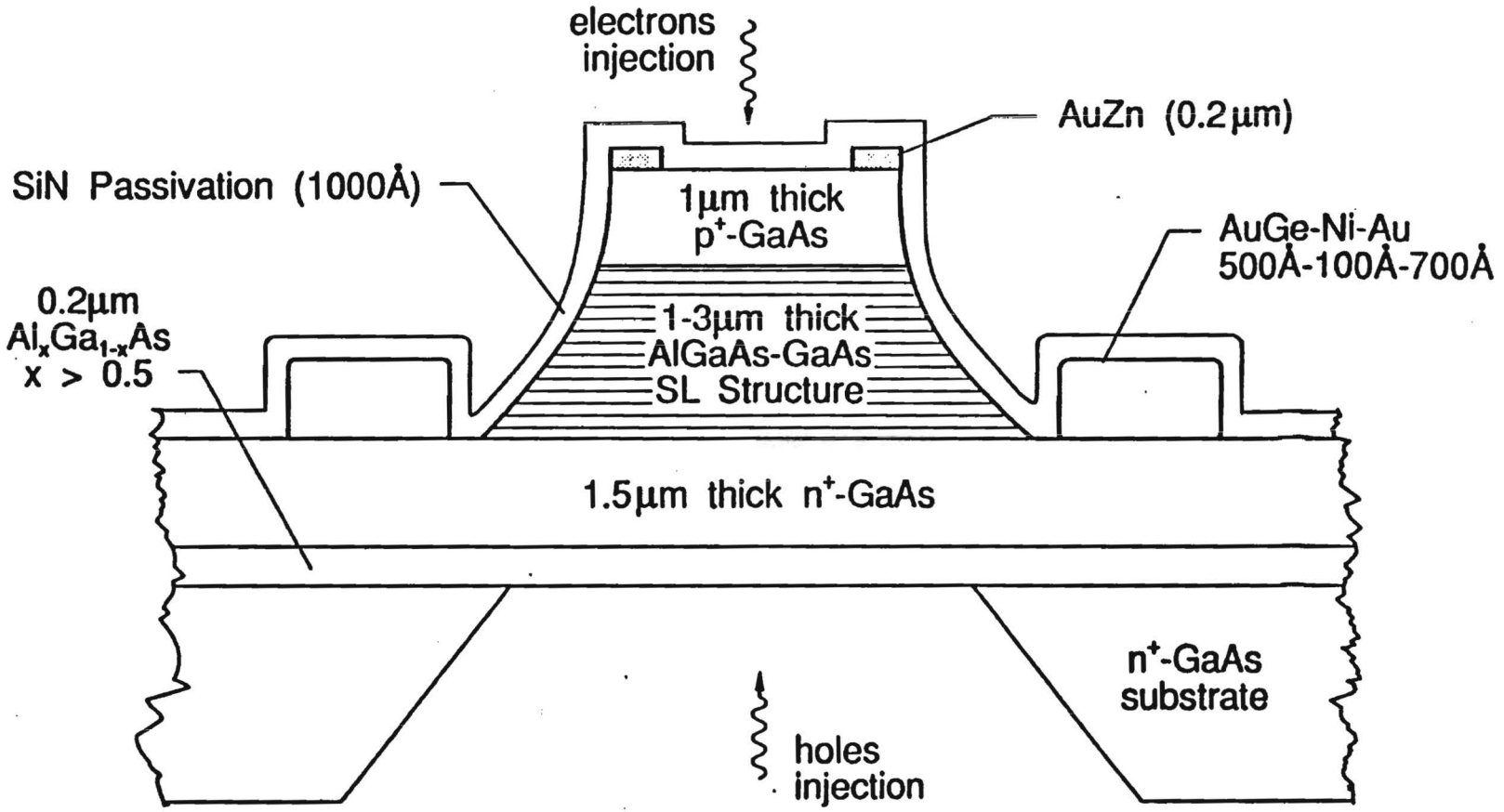

Superlattice Avalanche Photodiode Structure.

APPENDIX II

CHARACTERIZATION OF THE SL APDs

I. Introduction

To evaluate the performance of the APDs, it was necessary to measure the avalanche gain, the excess noise factor and the quantum efficiency of the devices. The current gain, as a function of reverse bias voltage, was found from the I-V curves of the diodes measured both in the dark and under illumination by a He-Ne laser. The excess noise factor, as a function of the avalanche gain, was calculated by measuring the noise power of the device for different values of the diode bias voltage. The quantum efficiency is determined by measuring the photogenerated current by an illuminating beam of known intensity under low bias voltage condition.

A. Description of the Optical Apparatus

The apparatus for the optical characterization has been configured to provide flexibility and reproducibility in the measurements. The optical source and accessories were mounted on an optical table and the power level of the laser beam was adjusted with an attenuator and neutral density filters. Figure 1 shows the complete optical system. The laser beam was split into two beams with a beam splitter and both beams were focused to the same point on the top of the microscope on either side of the diode box. The diode box contains the photodiode and the accompanying

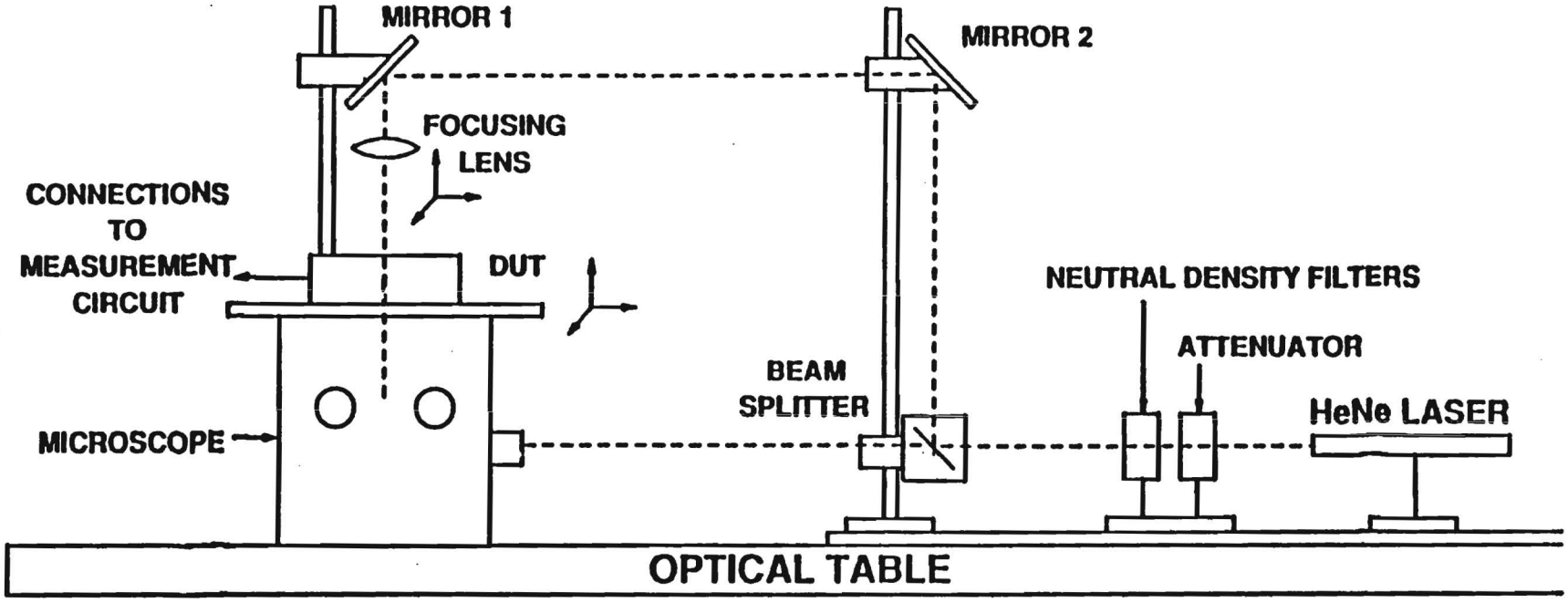

Figure 1. Optical Apparatus.

electrical circuit. The box has a hole on the top for illuminating the top side of the photodiode, and another hole on the bottom for illuminating the back side of the photodiode. The XYZ stage of the microscope was used for positioning the photodiode in the illuminating beam. A tungsten light placed in the microscope optical path instead of the laser was used for this purpose. The laser beam that goes through the microscope was focused with a 40X long focal length objective onto the photodiode with a 5 μm beam spot diameter. This small spot size was used to scan the active area of the photodiode to detect any non-uniformity in the light injection.

B. Description of the Electrical Circuit

The photodiode was mounted in a 8 pin dual-in-line package and inserted into the circuit showed in Figure 2. To permit the back side illumination, a hole of 20 mil diameter was laser drilled in the center of the package. The electrical circuit of the photodiode was divided into two parts to perform the following dc and ac measurements:

1. Current-voltage measurements were performed with the dc part of the circuit. The diode was connected in series with a precision resistor which provides a high input impedance to the ac circuit. The diode and the resistor were reverse biased with a battery that supplied a voltage selectable to within 2mV. The diode voltage bias then was the voltage dropped measured across the precision resistor. The selectivity of the system provides an

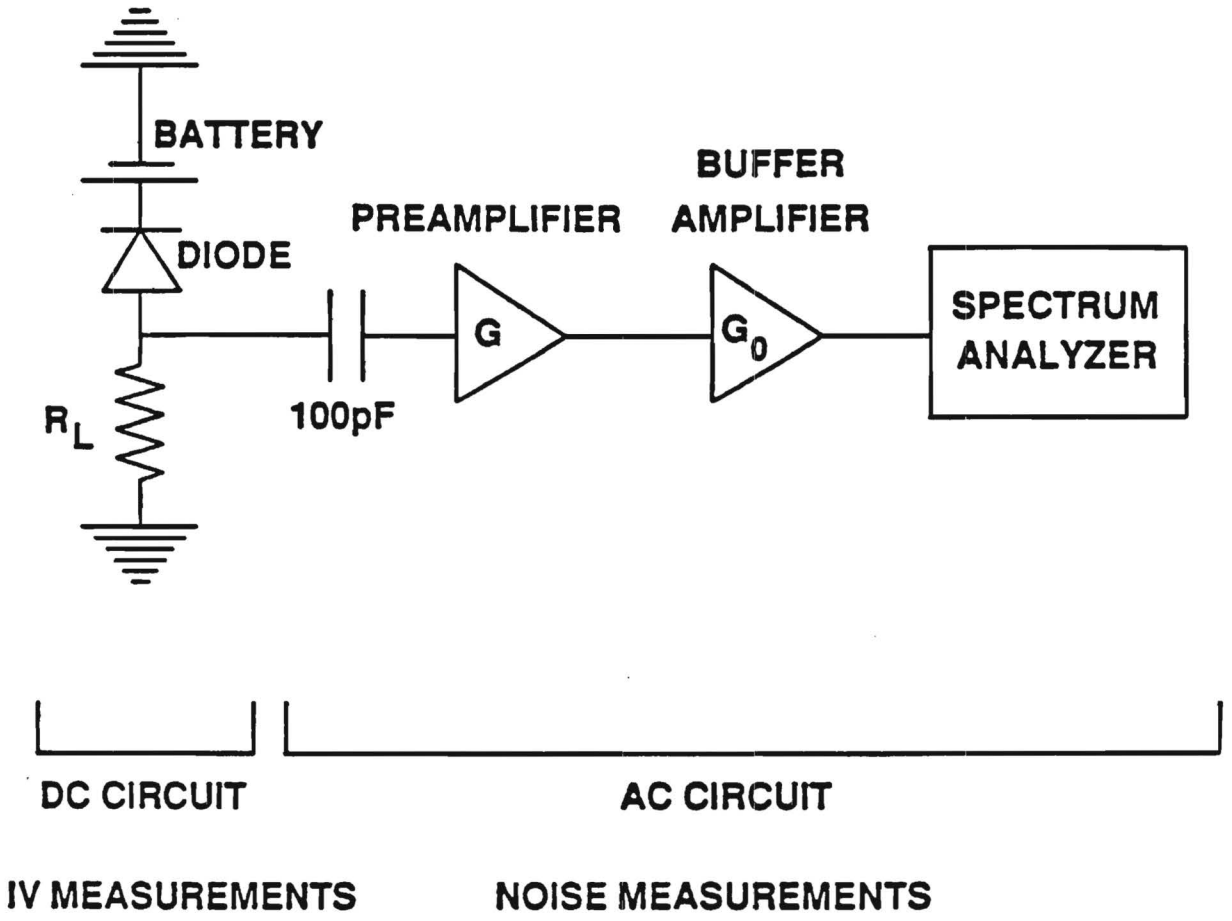

Figure 2. Diode Characterization Circuit

accuracy of 2pA in the bias current.

2. Absolute noise measurements were performed using the ac part of the circuit. The photodiode noise signal was coupled through a 100pF capacitor to a low noise preamplifier and the power of the amplified signal was measured on a spectrum analyzer at a fixed center frequency within a selected bandwidth. This frequency was chosen between 200 kHz and 300 kHz to avoid interferences with the 1/f noise of the photodiode. The measured power is the total output noise power of the circuit which includes the avalanche noise of the diode, the thermal noise of the diode series resistance and the load resistor, and the noise of the preamplifier. The preamplifier was chosen to provide a low noise with a medium input impedance (1 Kohms - 1 Mohms) in the frequency range of the measurements. A buffer amplifier was also added to the circuit in order to match the low output impedance of the preamplifier (1 Kohm) to the low input impedance of the spectrum analyzer. The equivalent electrical circuit is presented in Figure 3, where i^2 is the noise current source of the photodiode,

C_D is the photodiode capacitance,

R_D is the photodiode series resistance with $10 < R_D < 10^3$

e^2_D is the thermal noise of the diode resistance,

e^2_L is the thermal noise of the load resistor,

C_A is the input capacitance of the preamplifier,

R_A is the input resistance of the preamplifier and,

e^2_A and i^2_A are respectively the noise voltage and noise

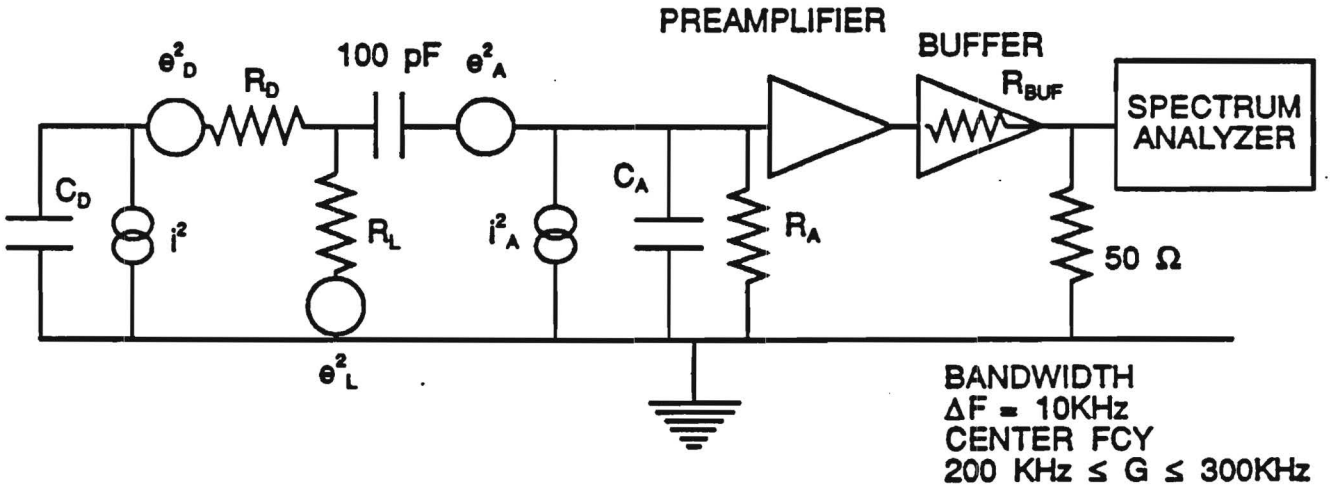

Figure 3. Equivalent Electrical Circuit

current source of the preamplifier.

C. Description of the Instruments

All the instruments used in the measurements were chosen based on noise considerations. The bias voltage supply, the voltmeter and the picoameter were battery powered in order to avoid the difficulty of rectifying noisy line voltages (120 V). From the previous description, the most critical instruments of the circuit were the low noise preamplifier and the spectrum analyzer. The Princeton Applied Research (PAR) preamplifier model 5004 was chosen for its low noise characteristics and compatible bandwidth of 0.5Hz - 1MHz. The spectrum analyzer had to meet the following requirements in order to obtain accurate noise measurements: a synthesized source stabilized to the center frequency of the measurements with a resolution bandwidth of <10 Khz, and a noise power accuracy of plus or minus 0.1 dBm. The Hewlett Packard model 8568B meets these specifications and was, therefore, used for these measurements.

II. Calibration of the Measurement Circuit.

To insure proper operation of the measurements system, it was necessary to obtain a precise and complete calibration of the circuit. The calibration includes three parts. The first part was related to the accurate determination of the parameters of the circuit presented previously in Figure 3. The second part was related to the measurement of the noise power of the circuit (without the photodiode) for a series of load resistors. The plot of the noise power as a function of the resistor value was compared with the plot obtained from the known contour figure of the preamplifier. From the plots, the parameters of the circuit were verified and any additional anomalies detected. The third part was to measure the noise of a well known device. A Si PIN photodiode was chosen for this purpose.

Part 1. I-V Measurements and Multiplication Gain Calculation

The following parameters were measured:

1. Total gain of the combination preamplifier-buffer amplifier
2. Noise equivalent bandwidth of the spectrum analyzer
3. The buffer amplifier output resistance.
4. The input capacitance of the preamplifier.

Part 2. Calibration of Entire Measurement Circuit

The noise power was measured for various load resistors, between 10 ohms and 1.5 Mohms, at the input of the ac circuit. The

equivalent electrical circuit is presented in Figure 4. The theoretical equation of the noise power measured on the spectrum analyzer is

$$\text{PowerMeasured} = (G+G_o)^2 \frac{e^2_A + R^2 i^2_A + e^2_R}{(1 + 4\ R^2_E C_A^2 \pi^2 F^2)^2} * \frac{50}{(50 + R_{buf})^2} * B$$

where $G+G_0$ is the total gain of the circuit,

e^2_A and i^2_A are respectively the noise voltage and noise current sources of the preamplifier,

R_E is the parallel combination of the amplifier input resistor R_A and the load resistor R_L,

e^2_R is the noise voltage source of the precision resistor,

C_A is the input capacitance of the preamplifier,

R_{buf} is the output resistance of the buffer,

F is the center frequency of the measurements and,

B is the equivalent noise bandwidth of the measurements.

The measured values of the output circuit noise power were compared with the theoretical values calculated with the above equation. The values of the parameters determined in part A were, in addition to the factory noise contour figure of the preamplifier. As shown in Figure 5, the theoretical predictions are in agreement with our experimental results.

A. Calibration Circuit

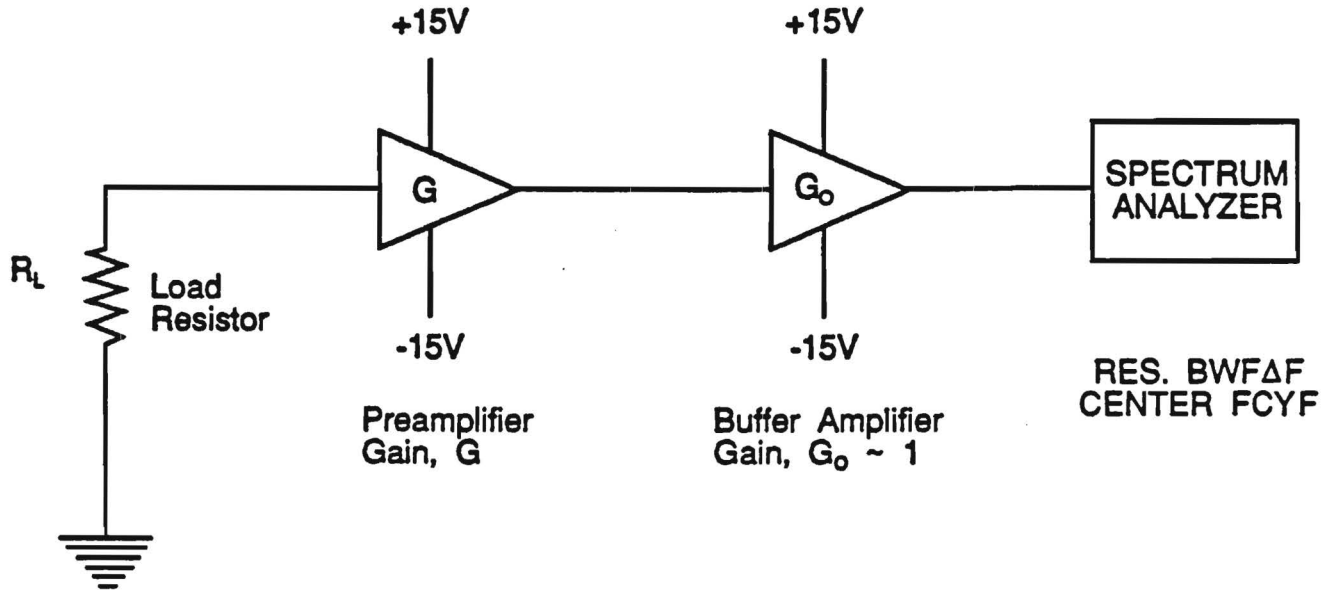

B. Equivalent Circuit

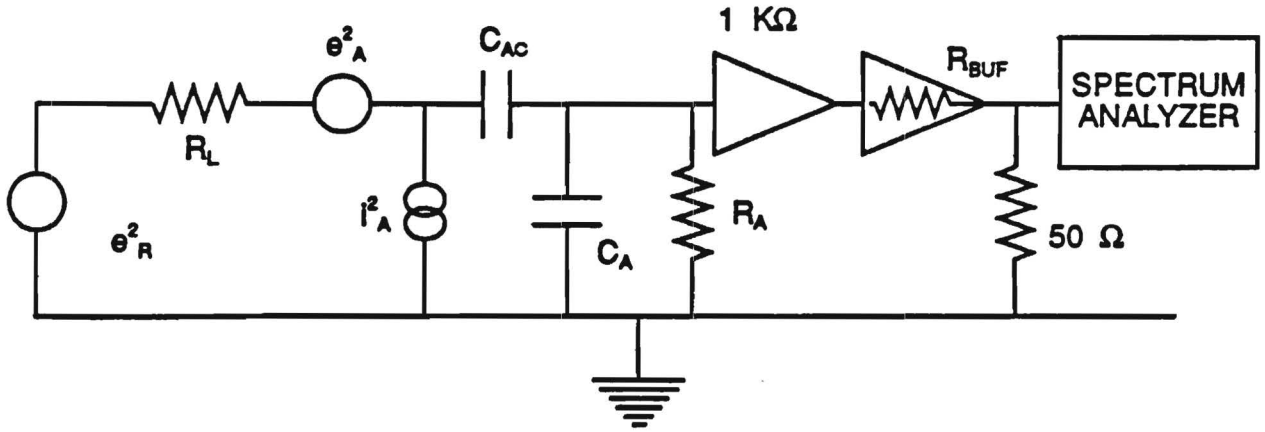

Figure 4. Equivalent Electrical Circuit for Calibration of Measurement System.

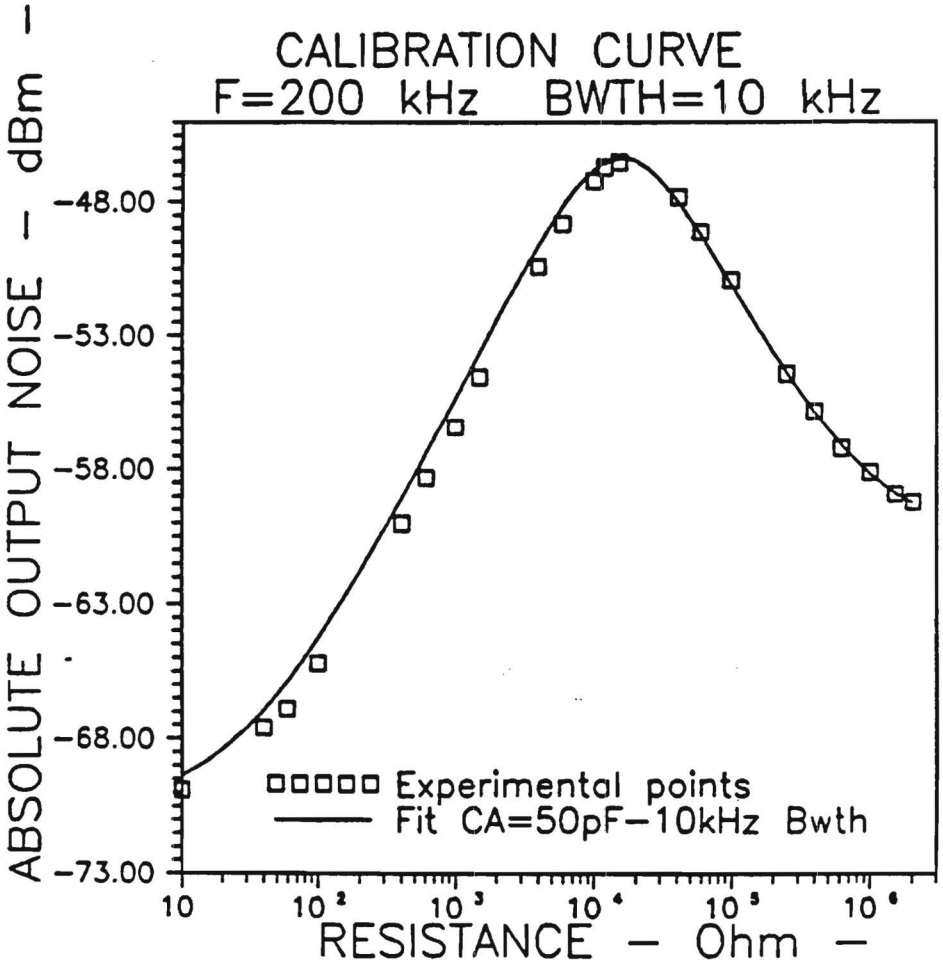

Figure 5. Output Noise for Various Resistors-Theoretical and Experimental Results.

Part 3. Calibration Using a Si PIN Photodiode

The photodiode chosen for a test calibration was a Si PIN photodiode model S1190 from Hamamatsu. Noise measurements were performed for diode bias voltages of 5 volt and 8 volt.

The results shown in Figure 6 represent the variation of the output circuit noise for increasing photocurrent at a constant diode bias voltage. At a constant bias, the output noise increased linearly with the current. The gradient of the output noise is proportional to the ratio of the photodiode shot noise current over the photocurrent, according to the relationship:

$$g = \frac{2 * q * I_{ph} * B}{I_{ph}} * (G+G_O)^2 * \frac{50}{(50+R_{buf})^2} * |Ze|^2$$

where g is the gradient of the output noise, q is the coulomb charge of a carrier, Z_e is the equivalent impedance of the circuit, I_{ph} is the photocurrent, and $2 * q * I_{ph} * B = \langle i^2 \rangle$ is the mean square shot noise value.

The PIN photodiode exhibited only shot noise at 5 or 8 volts, because there was no current gain. In Figure 6, the intercept of the linear fit with the y-axis represents the noise of the circuit itself including the preamplifier noise, the thermal noise of the diode resistance and the thermal noise of the load resistor.

C-V measurements were performed to accurately measure the capacitance of the diode at these two voltages. Then using the theoretical circuit equation, the value of the gradient, g, was

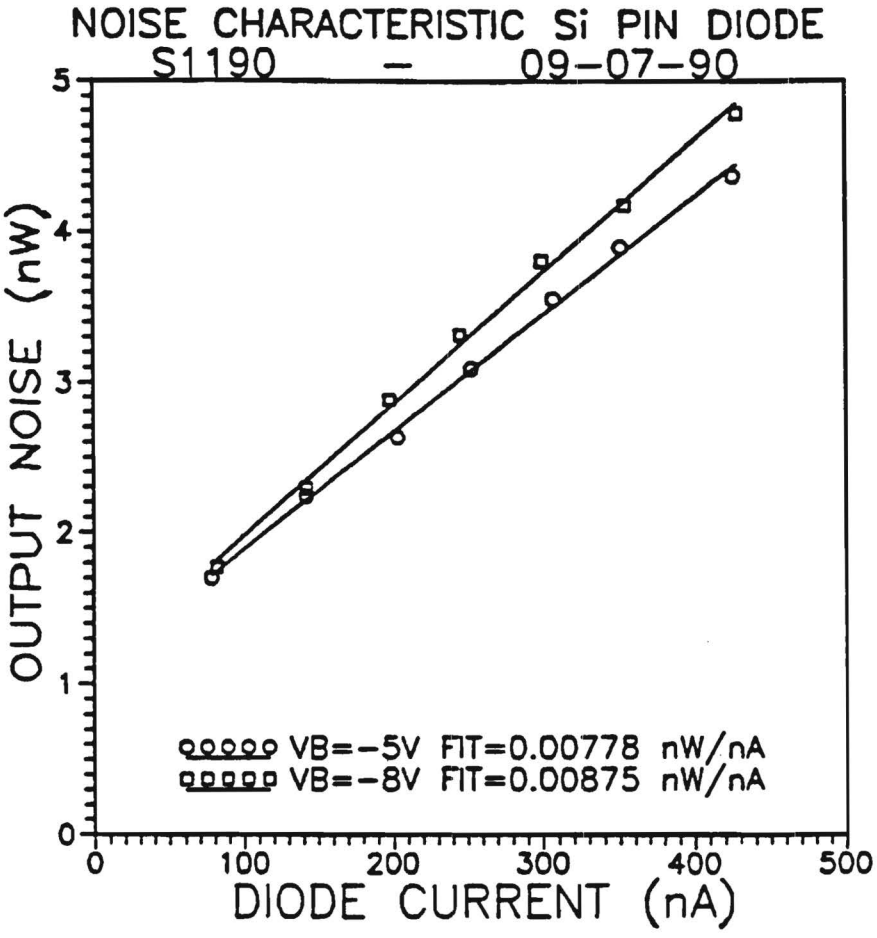

Figure 6. Output Noise Measured for a Si PIN Photodiode.

calculated and compared to the experimental value. For both bias voltages, the experimental results were within 0.5 % of the theoretical calculation. This last step confirmed that the calibration of the circuit was complete and that the noise measurement circuit was sensitive enough to measure the absolute noise of the SL APDs.

III. Theory of the Measurements

The measurement procedure developed to characterize the APDs can also be divided in three steps: I-V measurements and avalanche gain calculation, excess noise factor determination, and quantum efficiency calculation.

A. I-V Measurements and Multiplication Gain Calculation

To determine the avalanche gain of the photodiode, it is necessary to know the pure photocurrent injected after absorption of incident photons. The pure injected photocurrent is obtained by subtracting the I-V characteristics of the diode in the dark, from those obtained when the diode is illuminated by of a He-Ne laser.

The I-V measurements were performed with the dc part of the circuit presented in Figure 2. The current generated under the dark condition was first measured as a function of the total bias voltage. The total bias of the circuit was increased in multiples steps of 0.02 times the value of the breakdown voltage of the diode (from zero volt to the critical voltage value where the diode bias has reached the breakdown voltage). The bias current was always maintained below 1.5 μA to protect the device from being destroyed. The same measurements were then performed for photodiode illuminated with a He-Ne laser. The optical power of the laser beam was set at zero bias voltage to obtain less than 100 nanoamperes of photocurrent. This was done to avoid gain saturation of the photodiode.

For each series of I-V curves and at each value of the current

measured, the diode bias voltage is calculated by

$$V_d = V - R_L * I,$$

where I was the measured current, and R_L the value of the precision resistor in series with the diode.

A computer program was then used to separate the contribution of the dark current and the contribution of the photocurrent at each diode bias voltage. The pure generated injected, I_d, was thus plotted as function of the diode bias,

$$I_{ph} = I_{ph1}(V_d) - I_d(V_d),$$

where I_{ph} was the pure injected photocurrent at a diode bias voltage, V_d, I_{ph1} was the photocurrent measured at V_d on the picoammeter, and I_d is the dark current measured at V_d. The photocurrent variation at low bias voltage was then used to calculate the primary (or unmultiplied) photocurrent. The avalanche gain was plotted as a function of the diode bias voltage by taking the ratio of the photocurrent over the primary photocurrent,

$$M\ (V_d) = I_{ph}(V_d) \ / \ I_{po},$$

where M was the gain obtained at a diode bias voltage V_d, I_{ph} was the pure induced photocurrent at V_d, and I_{po} was the primary photocurrent.

B. Determination of the Excess Noise Factor

The excess noise factor is a measure of the increase of the

shot noise of the photodiode due to the multiplication process. It is calculated from measurements of the circuit output noise power versus the photocurrent for a constant diode bias voltage, i.e. a constant gain.

At a constant diode bias voltage, the circuit output noise power was first measured for increasing values of the photocurrent. The value of the photocurrent was changed by increasing the intensity of the laser light. Thus, for each photocurrent setting, the applied voltage V had to be changed to keep the diode bias voltage constant. V has to satisfy the relation,

$$I = (V - V_d) \; / \; R_L,$$

where I was the measured photocurrent, V was the applied bias voltage, V_d is the diode bias voltage, and R_L is the resistor in series with the diode.

The measurement procedure was repeated for different values of diode gain. At a constant gain, the output noise power is a function of the mean square diode current,

$$< i^2 > = 2 * q * I_{pO} * M^2 * F(M) * B$$

where I_{p0} is the primary photocurrent, M is the diode gain, q is the coulomb charge, B is the equivalent noise bandwidth, and F(M) is the excess noise for a gain M.

If Z_e is the equivalent circuit impedance, the output noise power measured was proportional to $< i_2 > * Z_e$. All the measured values fall on a line which has a slope equal to P over I_{ph} with

shot noise of the photodiode due to the multiplication process. It is calculated from measurements of the circuit output noise power versus the photocurrent for a constant diode bias voltage, i.e. a constant gain.

At a constant diode bias voltage, the circuit output noise power was first measured for increasing values of the photocurrent. The value of the photocurrent was changed by increasing the intensity of the laser light. Thus, for each photocurrent setting, the applied voltage V had to be changed to keep the diode bias voltage constant. V has to satisfy the relation,

$$I = (V - V_d) \; / \; R_L,$$

where I was the measured photocurrent, V was the applied bias voltage, V_d is the diode bias voltage, and R_L is the resistor in series with the diode.

The measurement procedure was repeated for different values of diode gain. At a constant gain, the output noise power is a function of the mean square diode current,

$$< i^2 > = 2 * q * I_{pO} * M^2 * F(M) * B$$

where I_{p0} is the primary photocurrent, M is the diode gain, q is the coulomb charge, B is the equivalent noise bandwidth, and F(M) is the excess noise for a gain M.

If Z_e is the equivalent circuit impedance, the output noise power measured was proportional to $< i_2 > * Z_e$. All the measured values fall on a line which has a slope equal to P over I_{ph} with

shot noise of the photodiode due to the multiplication process. It is calculated from measurements of the circuit output noise power versus the photocurrent for a constant diode bias voltage, i.e. a constant gain.

At a constant diode bias voltage, the circuit output noise power was first measured for increasing values of the photocurrent. The value of the photocurrent was changed by increasing the intensity of the laser light. Thus, for each photocurrent setting, the applied voltage V had to be changed to keep the diode bias voltage constant. V has to satisfy the relation,

$$I = (V - V_d) / R_L,$$

where I was the measured photocurrent, V was the applied bias voltage, V_d is the diode bias voltage, and R_L is the resistor in series with the diode.

The measurement procedure was repeated for different values of diode gain. At a constant gain, the output noise power is a function of the mean square diode current,

$$< i^2 > = 2 * q * I_{pO} * M^2 * F(M) * B$$

where I_{p0} is the primary photocurrent, M is the diode gain, q is the coulomb charge, B is the equivalent noise bandwidth, and F(M) is the excess noise for a gain M.

If Z_e is the equivalent circuit impedance, the output noise power measured was proportional to $< i_2 > * Z_e$. All the measured values fall on a line which has a slope equal to P over I_{ph} with

$$\frac{P(VD,M)}{I_{ph}} = \frac{\langle i_2 \rangle * |Z_e|^2}{I_{pO} * M} = 2 * q * F(M) * |Z_e|^2 * B * A$$

and

$$A = (G+G_O)^2 * 50 / (50 + R_{buf})^2,$$

where F is the excess noise factor for a gain M, and Z_e is the circuit equivalent noise bandwidth. When the diode has no gain, the mean square diode current becomes equal to the well known shot noise equation,

$$< i^2 > = 2 * q * I_{pO} * B$$

and the ratio of P (Vd,M) over I_{ph} becomes

$$\frac{P(Vd,1)}{I_{ph}} = \frac{< i^2 > * |Z_e|^2}{I_{pO}} = 2 * q * B * |Z_e|^2 * A$$

From the previous equations, the excess noise factor F(M) is defined by the relation

$$F(M) = \frac{P(Vd,M)}{I_{ph}} * \frac{I_{pO}}{P(Vd,M)} * \frac{1}{M}$$

To verify the measurement accuracy, the experimental value of P (Vd,1) over I_{p0} is compared to its theoretical value 2 * q * B * Z^2_e with Z_e, the equivalent circuit impedance defined by

$$Z_e = (Z_A // (Z_{AC}+R_L // (R_D+Z_{CD}))),$$

where Z_A is the preamplifier input impedance, Z_{AC} is the impedance of the coupled capacitance, R_D is the resistance of the diode, and

Z_{CD} is the capacitance of the diode. When Z_{CD} is higher than 2 Pf and changes with the diode bias voltage, Z_e also changes. Thus an accurate knowledge of the photodiode C-V characteristic becomes necessary as the calculation of F(M) will have to take into account the change of Z_e.

C. Quantum Efficiency Measurements

The quantum efficiency is defined as the number of electron-hole pairs generated per incident photon and, thus, is the quantity used to evaluate the sensitivity of the photodiode. The quantum efficiency, n_L, is by definition

$$\eta = (I_p/q) \; / \; (P_{opt}/hv),$$

where I_p is the photogenerated current by the absorption of incident optical power, P_{opt}, at a wavelength, (corresponding to a photon energy h√). In these studies the optical power was measured using a calibrated silicon model 818-ST detector from Newport. The optical power, P_{opt}, was measured at a low diode bias voltage, so that the current was still unmultiplied. The quantum efficiency η was then calculated using the previous equation.